Journal of Sound and Vibration (1994) **174**(1), 69–90

VIBRATION AMPLITUDES CAUSED BY PARAMETRIC EXCITATION OF CABLE STAYED STRUCTURES

J. L. LILIEN

University of Liège, Institut d'Electricité Montefiore, Sart Tilman (B28), B4000 Liège, Belgium

AND

A. PINTO DA COSTA

Instituto Superior Técnico DECivil, Avenida Rovisco, 1096 Lisboa Codex, Portugal

(*Received* 5 *May* 1992, *and in final form* 25 *January* 1993)

There are very impressive projects today for very long free span bridges, both for suspended (the Great Belt in Denmark—free span of 1624 m, Akashi Kaikyo in Japan—1990 m) and stayed bridges (the Pont de Normandie in France—free span of 856 m). Numerous wind and aerodynamic aspects have been taken into account [1]. However, this is not the case for the dynamics of cables. This paper deals with one kind of cable vibrations: the ones caused by parametric excitation (i.e., a dynamic instability of the cables due to small periodic movements of the girder and/or the masts). The approach is oriented to calculating the amplitudes and the mechanical tension oscillations. Amplitude formulae for transient as well as for steady state regimes are reviewed and/or deduced. Several time history simulations from the finite element code are presented (displacement and cable tension) and discussed. Practical cases are also discussed. The analysis leads to large amplitude (15 m) oscillation of an inclined 440 m stay (the longer stay of the Pont de Normandie), causing tension oscillation close to 80% around the initial value when the girder and/or the mast produce a 10 cm excitation upon the chord line. In large span stayed bridges, parametric excitation will be very probable due to the presence of many low frequencies in the girder and in the cable stays. This implies new trends in the design of very large stayed bridges.

1. INTRODUCTION

Cable vibrations of cable stayed bridges have recently been observed in several countries [2–6]. In Belgium [5, 6] the two most outstanding cases were observed in Liège's province: the Ben-Ahin and Wandre Bridges (both during 1988, March and October respectively). Nine cables on the same side of the mast were vibrating with an amplitude of more than 1 m peak-to-peak, in the first mode. The wind was about 10 m/s, not exactly perpendicular to the bridge, and the stays were not yet in their final states (not yet injected with epoxy-brai in the sheath). The change of wind direction stopped the vibrations. On the Wandre bridge [6], amplitudes were more limited (about 30 cm peak-to-peak) and some second mode oscillations have been observed. Other incidents have been described in the literature [2, 5]. During Ben-Ahin's oscillations it was rainy, during Wandre's oscillations no rain was noticed. Amplitudes were variable with time and some beating phenomena were observed. It is relevant to note that the oscillation net (for which the wind comes from the bottom side) has only some stays in oscillation. However, this half of the bridge was

0022–460X/94/260069 + 22 $08.00/0

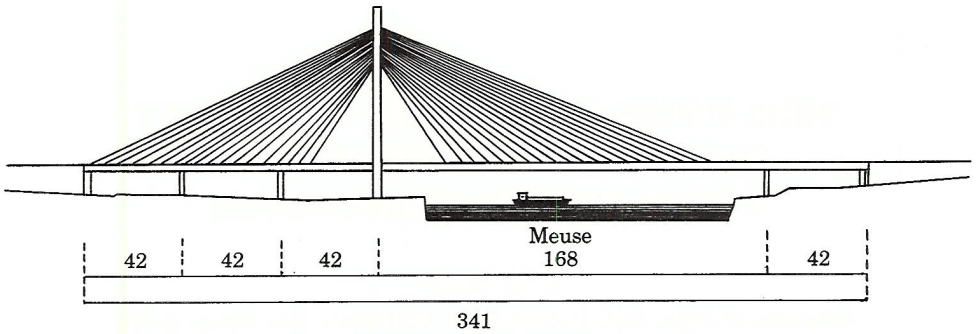

Figure 1. The Ben-Ahin bridge on the river Meuse in Belgium (dimensions in meters).

also just above the river Meuse, without any support for 168 (see Figure 1). Since 1988 the stays have been injected and no more oscillations have been observed.

Two explanations of this phenomenon could be given: (a) rain-wind induced galloping [2]; (b) parametric excitation of cables due to girder or mast oscillations [7–11].

(a) This explanation has been suggested by some Japanese authors [2], and it has been reproduced in laboratory tests. In fact, wind and rain, for a given wind orientation versus the stay and for a given range of wind speed, creates a water rivulet in the superior part of the stays. This profile asymmetry could induce lift forces (due to the aerodynamics of the new profile) and induce galloping instability (Den-Hartog galloping or flutter galloping). These phenomena are well known on other types of cables, such as overhead lines used for electrical energy transmission [12, 13].

(b) The girder or the masts might be excited [4] and could reach amplitudes of several centimeters. If these oscillations fall in certain ranges of frequencies, the cable movement can become unstable due to the non-linear effect known as parametric excitation: in fact, the movement of one cable end point induces a tension oscillation in the cable. This has some periodic effect on the stiffness which could induce, for some specific frequencies, very large movement. One should note that, whatever the excitation frequency is, one can observe the first mode oscillation of the cable. If the oscillation starts (depending on damping, frequency and end point(s) amplitude oscillation) the amplitude can reach a very large value which is almost independent of the damping. Only the non-linearities will limit its value. The unstable range of excitation increases very quickly with excitation amplitude, so that for large amplitudes of the end point oscillations, almost all of the frequency range becomes unstable (at least from about zero to about twice the first stay mode frequency).

This fact is of particular consequence for very large stayed bridges for which girder or mast oscillation frequencies are close to the stays' frequencies. For the same bridges large oscillations of the girder could be expected (about several centimeters, say, in the vicinity of a mid-span of a 900 m span seems to be very probable). If so, amplitudes of more than several meters could be observed in the stays, which will induce large tension oscillations and large corresponding dynamic stresses in some local girder positions. Tension oscillations will cause bending moment fluctuations in the girder which could exceed the static tension in some situations, especially during the erection stage. Amplitude oscillations could cause fatigue and contact between stays.

In the past, cable stayed bridge design has been based mainly on static considerations. However, the evolution in design techniques and materials have yielded the possibility for longer spans and more slender structures. Consequently, there are and will be bridges that during their lifetime (if not during their erection stage [4]) may be excited by the wind, due to their low vibration frequencies.

2. STATE OF THE ART

Galloping is well known, both theoretically and experimentally (see references [12, 13 and the references therein). Application to rain-wind induced galloping necessitates aerodynamic experiments, which have been carried out [2]. This phenomenon needs rain to occur, and this has not always been observed during some observations (e.g., the Wandre bridge). However, it is surely a good explanation for some cases.

In respect to parametric oscillation, the mathematical background is based on the Mathieu or Hill equation, about which numerous books and papers have been written [14–16]. Close connections with cables have been investigated [7, 9, 10, 11, 17–21]. Kovács [7] pointed out the danger of instability when the girder or mast frequency is close to twice a cable frequency; he also gave an instability condition as well as a simplified formula for the maximum amplitude. Tagata [18] studied the first mode parametric excitation and derived a non-dimensional non-linear Mathieu equation for the movement at mid-span of a weightless string. Labeeuw [8] gave minimal values for cable damping to avoid instability due to a time variable cable tension (he introduced the possibility of instability caused by the mixing of two different frequencies in the excitation). Takahashi [17] calculated the instability boundaries of the main instability regions of the Strutt diagram. Takahashi used the eigenvalue method for that purpose. Hsu [9] and Szemplińska-Stupnicka [19] have made two important advances in the knowledge of the mathematics of systems of equations with periodic coefficients. The first of these authors established the instability criteria for the fundamental instability regions.

3. INSTABILITY CONDITIONS

3.1. SEVERAL TYPES OF INSTABILITIES

The Mathieu differential equation governing the transverse ($w(x)$) movement of a cable [17, 22] subjected to anchorage periodic relative movement can be solved by the method of separation of variables in the form

$$w(x, t) = \sum Y_i(t) W_i(x), \tag{1}$$

where $W_i(x)$ is the ith modal shape and $Y_i(t)$ its corresponding amplitude (a list of symbols is given in the Appendix). Through the application of Galerkin's method to the governing equation one obtains a second order differential equation system with periodic coefficients for the modal amplitudes. As in reference [19], if one takes into account the viscous damping effects, one obtains

$$\mathbf{A}\ddot{\mathbf{Y}} + \mathbf{C}\dot{\mathbf{Y}} + [\mathbf{K} + \mathbf{P}(t)]\mathbf{Y} = \mathbf{F}(t), \tag{2}$$

where

$$\mathbf{P}(t) = \sum_{s=1}^{S} \mathbf{P}_s \cos 2\nu_s t. \tag{3}$$

The most simple case of parametric excitation is

$$\mathbf{P}(t) = \mathbf{P} \cos 2\nu t: \tag{4}$$

that is, $\mathbf{P}(t)$ is a single harmonic function. The general case of equations (2) is a set of *coupled* Mathieu equations. **A**, **C** and **K** are the real, symmetric and positive definite mass, damping and stiffness matrices, respectively. $\mathbf{P}(t)$ contains the excitation of the system. A fundamental non-dimensional parameter (introduced by Irvine [22, 23]) is the so-called λ^2

(see formula (17)) that quantifies the relative importance of elastic and geometric effects in the cable behaviour. If λ^2 is small (less than about 0·1, which means that the sag/span ratio is lower than 0·003) one must use for $W_i(x)$ the eigenfunctions of the taut string problem (this is the case for stayed bridges). In this case system (2) becomes uncoupled [24]. If λ^2 is not small the coupling is not negligible (this is the case for overhead electrical lines [12]). This has some effect on the consequent types of instability and the sharpness of instability regions (given by the Strutt diagram) [17, 19].

If ω_s is one natural frequency of a cable (mode s) instability can occur in the neighbourhood of the following excitation frequencies.

(a) For simple parametric resonance these frequencies are

$$\omega_{exc} = 2\nu = 2\omega_s/k \qquad \text{for all } k; \quad s \text{ integer:} \tag{5}$$

thus for $2\omega_1$, ω_1, $(2/3)\omega_1$, $(1/2)\omega_1$, $(2/5)\omega_1$, etc., if one considers only the first mode. It is quite surprising to realize that close to zero frequency (k high) the instability still exists. The influence of damping will clarify this fact.

(b) For combination parametric resonance (interaction between some modes) the frequencies are

$$\omega_{exc} = 2\nu = (\omega_s \pm \omega_t)/k, \qquad \text{for all integer } k, \qquad s, t \text{ odd integers.} \tag{6}$$

This gives the same values as for (a) because for stayed bridges (small λ) $\omega_k = k\omega$. The consequence of the uncoupling of equations (2) is the non-existence of combination parametric resonance.

As shown in references [22, 23] the ω_s are the roots of the transcendental equation

$$\operatorname{tg}(\Omega_s/2) = (\Omega_s/2) - (4/\lambda^2)(\Omega_s/2)^3, \qquad \text{where } \Omega_s = \omega_s l/\sqrt{T_0/m}. \tag{7}$$

For small λ^2 (this is the case for stayed bridges, except for the longer stays of very large bridges) equation (7) gives, (for the case of λ^2 not small, interpolation from the tables of reference [22] may be carried out)

$$\omega_s = (s\pi/l)\sqrt{T_0/m} = s\omega_1, \tag{8}$$

where l is the chord length, m is the mass per unit length, T_0 is the static tension and s is the mode number (or the number of loops in the span for the corresponding oscillation frequency). As a quantitative estimate of the effect of λ on large stayed bridges, one can consider the longer stay of the Pont de Normandie, which is about 440 m in length; for this case λ is close to 1·77 and there is an upper shift of the first mode frequency of about 6·9% compared to that given in formula (8).

The parameter space of a simple Mathieu equation (the first mode) with a qualitative scheme for unstable regions is represented in Figure 2. The damping has an erosion effect on the boundaries of instability regions: the greater the damping the greater the excitation needed to cause instabilities. This will be quantified hereafter, but one can imagine that this erosion effect is more significant the narrower the instability region [25].

Ultra-harmonic parametric resonance ($k > 2$) has a narrow band of instability, except for very large bridges with large excitation amplitudes. In fact one can establish the minimum excitation amplitude which is needed to start the instability [8, 26]:

$$X_d/X_0 = \Delta T/T_0 = 2\sqrt{[1 - (\omega_{exc}/2\omega_1)^2]^2 + (\delta/\pi)^2(\omega_{exc}/2\omega_1)^2}, \qquad \text{with } \omega_{exc}/\omega_1 \approx 2. \tag{9}$$

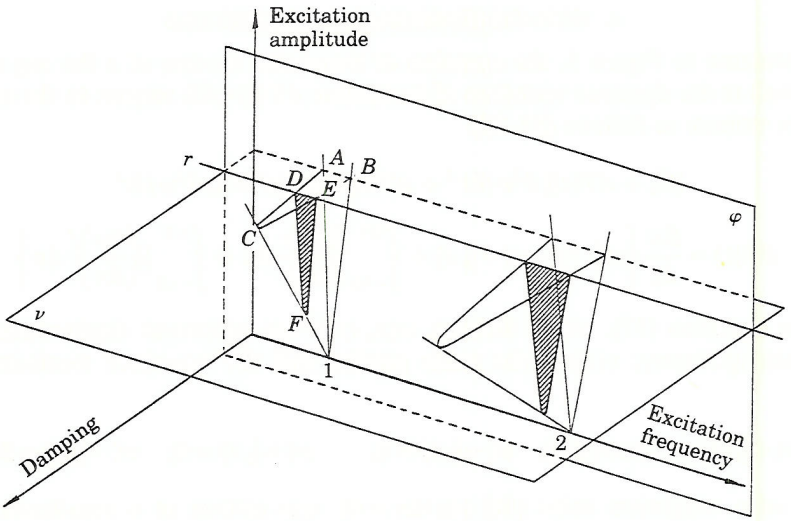

Figure 2. Instability regions, qualitatively drawn in the Mathieu equation parameter space.

This is because for small oscillation (the situation at the onset of an instability), one can write, for stayed bridges (which have a very low λ Irvine parameter), $\Delta T = (EA/L)X_d$. Labeeuw [8] considered another kind of instability which needs some other type of excitation, but is a very practical one: this is due to a mixture of two or more harmonic functions (several girder modes could be excited together by the wind). It can be proved in this case that some new instability regions will appear in the range (remember that ω is the half excitation frequency): $\nu_i + \nu_j = \omega_k$.

3.2. HOW TO COMPUTE THE INSTABILITY REGIONS

There are two ways to find the instability regions (in the frequency–excitation plane, such as plane φ in Figure 3): (a) the harmonic balance method [10, 17] applied to the system of differential equations for the modal amplitudes to which instability criteria can be applied (investigating the structure of the eigenvalues), (b) an iterative procedure via Newton's method coupled with Floquet theory [16]. To establish the instability regions in the frequency–damping plane, (plane ν in Figure 4) one can use classical formulae (see equation (6) of section 4 of reference [8], and reference [26]) for single frequency excitation or and iteration procedure for two frequencies excitation (see equation (7) of reference [8].

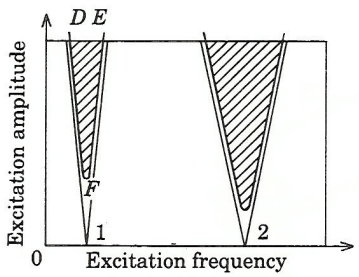

Figure 3. Section of Figure 2 on the amplitude–frequency plane. The shading denotes the unstable region.

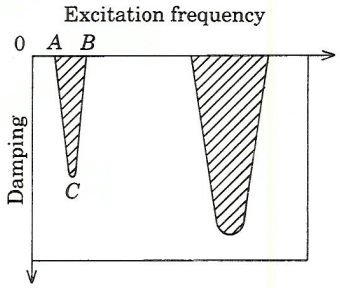

Figure 4. Section of Figure 2 on the damping–frequency plane. Key as Figure 3.

4. NON-DIMENSIONAL PARAMETERS

With reference to Figure 5, the equation of transverse motion of a flat sag suspended cable, as well as the dynamic variation of its tension $\Delta T(t)$ with respect to the static value T_0, can be written as follows [22, 23]:

$$[T_0 + \Delta T(t)]\,\partial^2 w/\partial x^2 + \Delta T(t)\,\mathrm{d}^2 z/\mathrm{d}x^2 = m\,\partial^2 w/\partial t^2, \tag{10}$$

$$\Delta T(t) = \frac{EA}{L_e}\left\{u(\tfrac{1}{2}, t) - u(-\tfrac{1}{2}, t) + \int_{-1/2}^{1/2} \frac{\mathrm{d}z\,\partial w}{\mathrm{d}x\,\partial x}\,\mathrm{d}x + \int_{-1/2}^{1/2} \tfrac{1}{2}\left(\frac{\partial w}{\partial x}\right)^2 \mathrm{d}x\right\}. \tag{11}$$

For L_e see equation (17), which follows; $w(x, t)$ is the transverse displacement relative to the static geometry; $z(x)$ is the static profile; and the boundary conditions of the cable are

$$u(+\tfrac{1}{2}, t) = X_d \cos(2vt), \quad u(-\tfrac{1}{2}, t) = 0, \qquad w(+\tfrac{1}{2}, t) = 0, \quad w(-\tfrac{1}{2}, t) = 0. \tag{12}$$

Thinking of a weightless cable [18] ($\mathrm{d}z/\mathrm{d}x = 0$), one arrives at a non-linear Mathieu differential equation for the first mode amplitude (Y),

$$\ddot{Y} + b\dot{Y} + \omega_1^2[1 + 2\xi \cos 2vt + \tfrac{4}{3}(Y/K)^2]Y = 0, \tag{13}$$

in which $\xi = X_d/2X_0$ (X_0 is the initial applied stretch and X_d is the driving amplitude) and

$$K = (4/\pi)\sqrt{X_0 l/3}, \tag{14}$$

l being the cable length and b being a damping coefficient. If one writes

$$v = Y/K, \qquad \tau = \omega t, \qquad k = b/\omega_1, \qquad a = \omega_1/v, \tag{15}$$

the following non-dimensional equation is obtained [18]:

$$v'' + kav' + a^2[1 + 2\xi \cos 2\tau + \tfrac{4}{3}v^2]v = 0. \tag{16}$$

Here the prime denotes the derivative with respect to τ. Therefore, there are three non-dimensional parameters, one for the excitation frequency (a), one for the excitation amplitude (ξ) and one for the damping (k). Since one is considering a taut cable, equation (16) is valid to a good approximation, for an inclined position of the cable (Y meaning the displacement orthogonal to the chord and v the corresponding non-dimensional value).

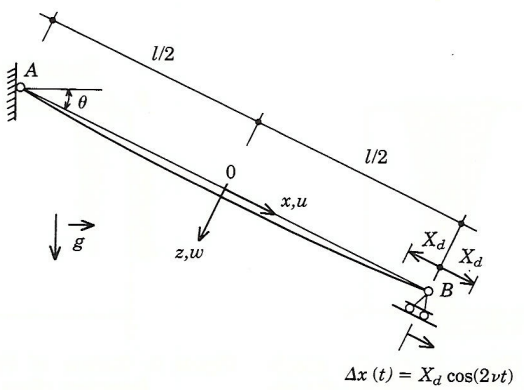

Figure 5. A typical cable stay and its boundary conditions.

Cable tautness (or flatness) can be measured through another non-dimensional parameter [22, 23]:

$$\lambda^2 = [mgl(\cos\theta)/T_0]^2 l/(T_0 L_e/EA), \qquad L_e = l\{1 + \tfrac{1}{8}[mgl(\cos\theta)/T_0]^2\}. \tag{17}$$

Here T_0, l and L_e are measured upon the chord line. λ^2 involves the cable elastic properties as well as its geometry. Cables of electrical overhead lines have a very large λ: that is, their response is mainly due to profile changes. On the other hand, cables of stayed bridges are associated with small λ^2, which means that their behaviour is governed by the extensibility of their material ($\lambda^2 \ll 4\pi^2$). Actually, the λ parameter is influenced by the stiffness of anchoring points of the cable [12] and L/EA must be replaced by $L/EA + (1/K_{mast} + (1/K_{girder})$.

In conclusion, the important non-dimensional parameters for stayed bridges are (taking into account that λ^2 is already fixed with a small value)

$$k = b/\omega_1 = \delta/\pi, \qquad \xi = X_d/(2X_0), \qquad a = \omega_1/v. \tag{18}$$

5. AMPLITUDES

5.1. THE STEADY STATE RESPONSE

The main parametric excitation region of the cable is to be considered. The limit cycle amplitude can be deduced by using the harmonic balance method; it is supposed for simple parametric excitation that even if the excitation frequency is $2\omega_1$, the sag oscillation will be at the frequency ω_1. Therefore the corresponding limit cycle oscillation is supposed to be of the form (phase shift unknown, thus both sin and cos must be included)

$$Y = A \sin\omega_1 t + B \cos\omega_1 t. \tag{19}$$

Substituting equation (19) into equation (13) yields

$$\begin{aligned}
&[-(bB/\omega_1) + (A^3/K^2) + (AB^2/K^2) - \xi A] \sin\omega_1 t \\
&\quad + [(bA/\omega_1) + (A^2B/K^2) + (B^3/K^2) + \xi B] \cos\omega_1 t \\
&\quad + [(1/K^2)\{-(A^3/3) + AB^2\} + \xi A] \sin 3\omega_1 t \\
&\quad + [(1/K^2)\{(B^3/3) - A^2B\} + \xi B] \cos 3\omega_1 t = 0,
\end{aligned} \tag{20}$$

in which the $3\omega_1$ terms will be neglected. The constants A and B can then be deduced from

$$\begin{aligned}
&(1/K^2)A^3 + (1/K^2)AB^2 - \xi A - (b/\omega_1)B = 0, \\
&(1/K^2)B^3 + (1/K^2)BA^2 + \xi B + (b/\omega_1)A = 0.
\end{aligned} \tag{21}$$

Suppose that the phase shift between the excitation (supposed to be $\cos 2\omega_1 t$) and the sag oscillation is close to $\pi/2$; this means $B \ll 1$, so that B^3 is negligible. Then, from the second of equations (21),

$$B = [-(b/\omega_1)A]/[(A^2/K^2) + \xi], \tag{22}$$

so that the first of equations (21) gives, if AB^2 is neglected,

$$A = (4/\pi)\sqrt{X_0 l/3}\sqrt[4]{(X_d/2X_0)^2 - (b/\omega_1)^2}, \tag{23}$$

or

$$A = (2/\pi)\sqrt[4]{(\tfrac{2}{3}X_d l)^2 - ((4/3\pi)(T_0 l^2/EA)\delta)^2}, \tag{24}$$

where $b = 2n_1\delta$ with $n_1 = \omega_1/(2\pi)$. Because $B \ll 1$, equations (23) and (24) lead to first mode amplitude oscillation of the cable. If $A = 0$, one can obtain the threshold excitation amplitude

$$A = 0 \quad \text{or} \quad (X_d/2X_0)^2 = (b/\omega_1)^2, \quad \text{or} \quad X_d/X_0 = (\Delta T/T_0) = (2/\pi)\delta = 2k. \tag{25}$$

This is a particular case of formula (9) that one can now rewrite by using the non-dimensional parameters as

$$\xi = \sqrt{[1 - (1/a)^2]^2 + (k/a)^2}. \tag{26}$$

However, the same formula gives access to a *limit cycle* non-dimensional amplitude (refer to equation (18) for the non-dimensional parameter definitions)

$$A/K = \sqrt[4]{\xi^2 - k^2}. \tag{27}$$

The dotted lines in Figure 6 show the corresponding curves for two different forms of damping. *Note that damping influences the point of onset but has no practical influence on the limit cycle values.* The physical explanation of this fact is related to the very low level of energy dissipation owing to inner damping of the cable (at this stage the aerodynamic damping has been neglected, so that the corresponding energy dissipation has nothing to

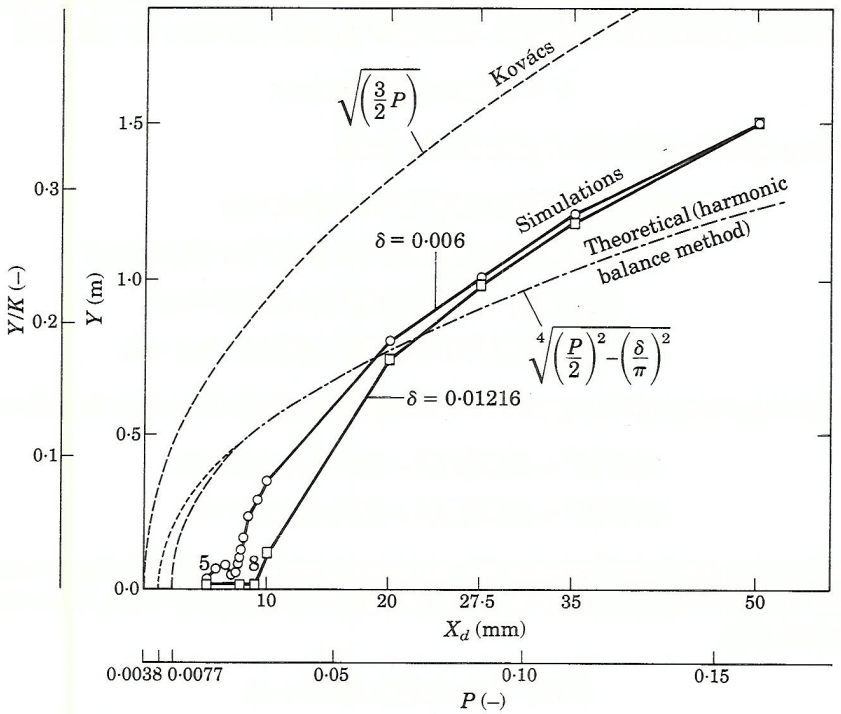

Figure 6. The general non-dimensional curve for any parametric excitation ($2\omega_1$); $\theta = 10°$. One theoretical curve gives the limit cycle values (peak-to-peak is $2Y$), the other theoretical curve is the maximal transient value, following Kovács [7], and the simulation curves are the computed ones, for the maximum peak value observed during the transient. Dimensional axes are for the specific case of the Ben-Ahin bridge. $P = 2\xi$.

do here with limit cycle amplitude; an evaluation of this effect will be quantified at the end of the paper). The physical reason for the amplitude limitation is explained after formula (30) which follows.

Note that this curve is independent of the structure (for small λ), so that it is easy to deduce one's own particular case: one has only to calculate one's own parameters. Some applications will be presented in the next section.

5.2. THE TRANSIENT BEFORE REACHING THE LIMIT CYCLE

Before reaching the limit cycle, some transient occurs which can last for several minutes, depending on the oscillation frequency(ies), the damping and the excitation amplitude. This transient is always of particular interest because it can induce amplitudes sensibly larger than during the limit cycle. In fact, tension oscillation in the cable is not symmetric about the initial value (see Figure 7). This non-symmetry will cause a shift in the oscillation frequency which has some influence on the amplitude. Moreover, there is a beating phenomenon between the basic frequency and the modified frequency until the final "lock in" on the limit cycle frequency.

The maximum maximorum amplitude of the first mode sag oscillation can be deduced from the expression for the tension, as given by Tagata [18] or by equation (11):

$$T(t) = T_0[1 + 2\xi \cos 2vt + \tfrac{4}{3}Y^2/K^2]. \tag{28}$$

If one now supposes that the answer can be expressed by (variable amplitude)

$$Y(t) = A(t) \sin \omega_1 t, \tag{29}$$

substitution into equation (28) gives

$$T(t) = T_0[1 + 2\xi \cos 2\omega_1 t + (4/3K^2)A^2(t) \sin^2 \omega_1 t],$$

in which the bracket $[\cdots]$ can be written as

$$1 + (2/3K^2)A^2(t) + [\{\Delta T_{max}/T_0\} - \{2A^2(t)/3K^2\}] \cos 2\omega_1 t. \tag{30}$$

The physical explanation is as follows. The maximum maximorum amplitude of oscillation can be reached when there is a complete and synchronous compensation between the elastic elongation of the cable and the displacement of the end point. This is the extreme case of total transfer of input energy into deformation energy. Hence at the maximum amplitude the tension oscillation will be close to zero, which means it will be roughly constant over all of one period of sag oscillation, but not around the initial value. For energy balance this constant value is around the maximum of the tension oscillation, where one can say that

$$T_{max} - T_0 = X_d EA/l, \qquad \text{or} \qquad T_{max}/T_0 = 1 + X_d/X_0. \tag{31}$$

In such conditions equation (30) leads to the maximum amplitude

$$(\Delta T_{max}/T_0) - (2A_{max}^2/3K^2) = 0, \qquad \text{or} \qquad A_{max} = (2/\pi)\sqrt{2lX_d}, \qquad \text{or} \qquad v_{max} = \sqrt{3\xi}. \tag{32}$$

From the same equation (30) one can also calculate an approximation to the range of tension oscillation *during the limit cycle*. In fact, during the limit cycle, the amplitude is (see formula (24) with $\delta = 0$)

$$A_{LC} = (2/\pi)\sqrt{\tfrac{2}{3}X_d l}, \qquad \text{or} \qquad v_{LC} = \sqrt{\xi}. \tag{33}$$

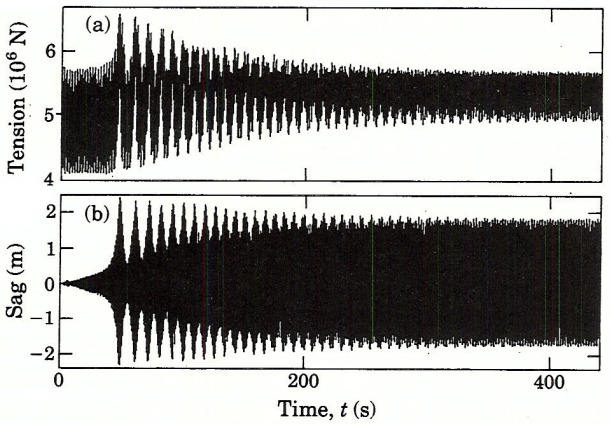

Figure 7. Parametric resonance at $2{\cdot}097\omega_1$ (Ben-Ahin bridge, $\delta = 0{\cdot}006$, excitation amplitude of 5 cm), with 450 s of simulation. See also Figures 9 and 10. (a) Tension oscillations (maximum × $1{\cdot}5\ 10^6$ N peak-to-peak); (b) sag oscillations (maximum 4·5 m peak-to-peak).

Substituting this in equation (30) yields

$$T(t) = T_0 + (\Delta T/3) + \tfrac{2}{3}\Delta T \cos 2\omega_1 t \qquad \text{in the range } [T_0 - \tfrac{1}{3}\Delta T,\ T_0 + \Delta T]. \tag{34}$$

By comparing this interval with the computer simulations (Figure 7) one concludes that the upper bound is correct but the lower bound seems to be closer to T_0 than to $T_0 - \Delta T/3$.

Classical resonance also deserves some comments. It is remarkable that it is more difficult to find (theoretically) the corresponding amplitude than it has been for parametric excitation! It is a matter of fact that the non-linearities also limit the amplitude. In fact, if one applies the simple formula deduced from linearized theory [8, see equation (6) of section 2.2], one obtains 14 m instead of 2·4 m (peak-to-peak) for the basic case treated in the simulations (see Figure 8).

6. COMPUTER SIMULATIONS AND PHYSICAL DISCUSSION

Numerical simulations have been carried out with SAMCEF-CABLE [27, 28], part of the general finite element software widely used today at more than one hundred industrial sites in Belgium and France. The basic hypotheses for SAMCEF-CABLE (statics and dynamics of cables) are as follows: no flexural or torsional stiffness considered; no internal damping; small deformations (but large displacements); isoparametric finite elements of different orders. Of course, elasticity is taken into account and many loadings are possible (local, distributed, wind, ice, gravity, electromagnetic, forced value, etc.). Viscous damping can be introduced in an artificial numerical way [27, 28]. The results of some of the simulations are presented in detail in Figure 8. All dots correspond to computed points.

The loading has been chosen as forced displacement in the chord direction of the cable. All simulations concern one loop oscillations (except for the case $3\omega_1$). The cable has been discretized into 12 first order cable elements.

As non-dimensional parameters have been used in the simulations, none of the results are for just a particular cable; only the parameters are important. For example, the inclination has no influence (this is because the λ Irvine parameter is very low). The

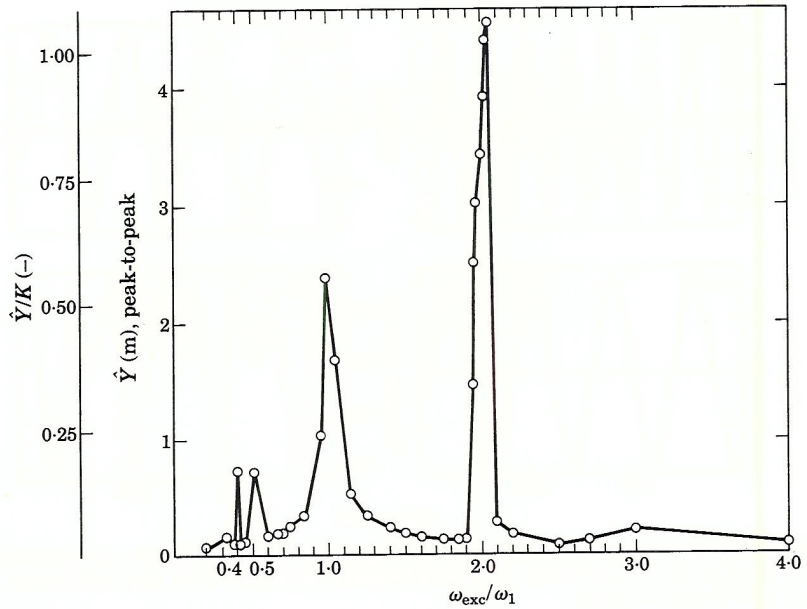

Figure 8. Peak-to-peak non-dimensional amplitude of one loop oscillation of a cable stay for different excitation frequencies with constant amplitude ($\xi = 0{\cdot}08$). For the practical case of one stay from the Ben-Ahin bridge the real amplitude of oscillation is also plotted; in this case the excitation amplitude is 5 cm. $\delta = 0{\cdot}006$, $X_d = 0{\cdot}05$ m, $T_0 = 4\,895\,190$ N, $A = 0{\cdot}00826$ m^2, $E = 210 \times 10^9$ N/m^2, $m = 64{\cdot}841$ kg/m, $\theta = 0°$; $l = 110{\cdot}505$ m.

damping range has been chosen in a practical range of modern stays (parallel wires [8, 29]): this means a logarithmic decrement of about 0·006. Another simulation with a double value has been performed to indicate the impact of this damping.

For a cable with properties similar to those of one of the Ben-Ahin bridge stays, a sequence of 36 computer simulations has been performed (Figure 8). The excitation amplitude was kept constant ($x = 0{\cdot}05 \sin 2vt$(m)) while the excitation frequency ($2v$) was varied in the range $0{\cdot}2\omega_1$–$4\omega_1$ with a greater refinement in the neighbourhood of main detected peaks.

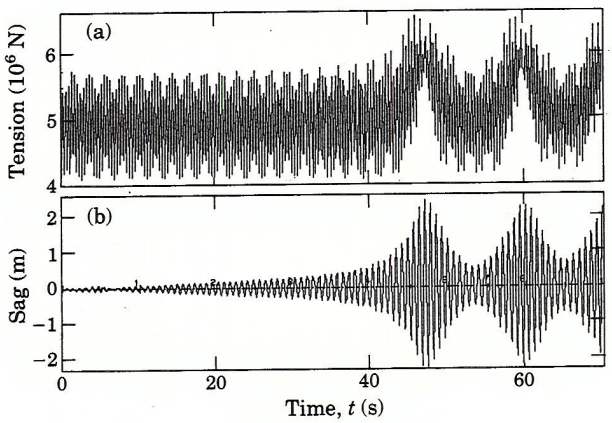

Figure 9. Detail of Figure 7 during the first 70 s. (a) Tension oscillations (max $1{\cdot}5 \times 10^6$ N peak-to-peak); (b) sag oscillations (max 4·5 m peak-to-peak).

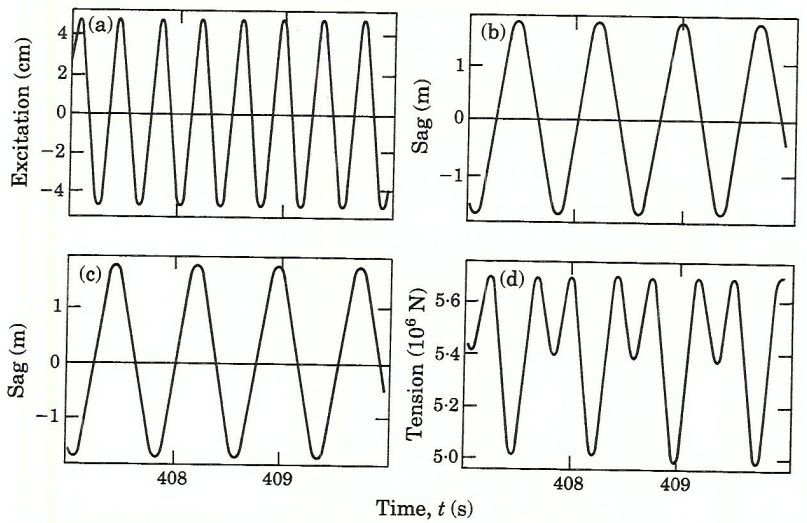

Figure 10. Detail (three last seconds of simulation) of Figure 7 during the limit cycle. (a) Excitation amplitude (10 cm peak-to-peak); (b) sag oscillation (3 m peak-to-peak); (c) same as (b) (sag oscillation); (d) tension oscillation (7×10^5 N peak-to-peak).

6.1. COMMENTS ABOUT THE COMPUTED RESULTS

(1) The results of parametric excitation at about twice the frequency of the one loop mode of the cable are shown in Figures 7, 9 and 10. It is of particular interest to note that, as discussed in the preceding section, the maximum amplitude is reached when the tension oscillation tends to zero around the maximum initial value. Moreover, the limit cycle tension amplitude is reduced by about 50% compared to the maximum value. Tension oscillation during the limit cycle is sensibly shifted from the initial oscillation.

Figures 11 and 12 are for the classical resonance at ω_1. Here one also observes a shift in the tension, but the oscillation still remains about constant around a variable mean value. The maximum amplitude is lower than with parametric excitation at $2\omega_1$, and much lower than according to linearized theory [8, see equation (6) of section 2.2].

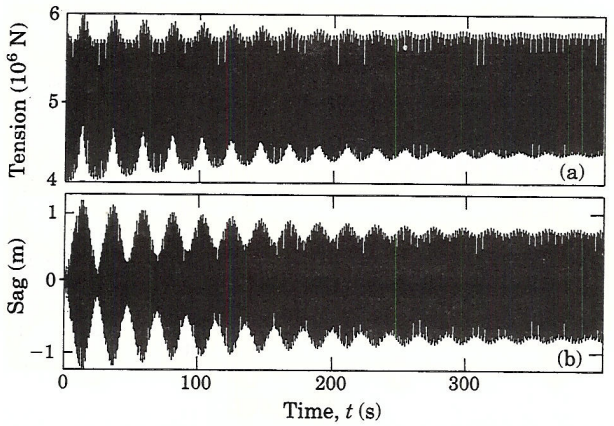

Figure 11. Simple resonance (Ben-Ahin bridge, $\delta = 0{\cdot}006$, excitation amplitude of 5 cm), with 400 s of simulation. (a) Tension oscillations (max 18×10^5 N peak-to-peak); (b) sag oscillations (max 2·4 m peak-to-peak).

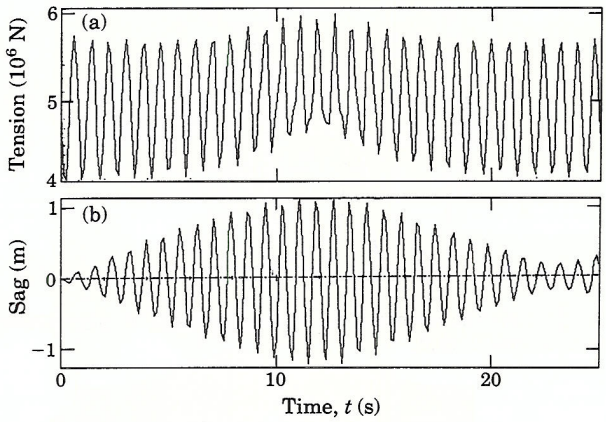

Figure 12. Detail of Figure 11 during the first 25 s. (a) Tension oscillations (max 18×10^5 N peak-to-peak); (b) sag oscillations (max 2·4 m peak-to-peak).

Another sequence of simulations that we have performed was to focus on classical parametric excitation ($2\omega_1$) with increasing amplitudes from very low to some centimeters, so that one could detect the starting points and the shapes of the curves. We did this for two values of the damping (see Figure 6).

(2) In Figure 8 the classical resonance and first parametric resonance regions are clearly visible (the two highest peaks). Some ultra-harmonic instability is clearly visible at 1/2 and 2/5 of the ratio ω_{exc}/ω_1. No other ultra-harmonic instability (2/3, 1/3, etc.) (see formula (5)) has been observed; this is due to the damping ($\delta = 0{\cdot}006$) and excitation amplitude (5 cm) values used.

(3) In Figures 13 and 14 one can observe that for $X_d = 0{\cdot}05$ m, the maximum amplitude observed between the boundaries of the instability region occurs for $2{\cdot}097\omega_1$ (on the right

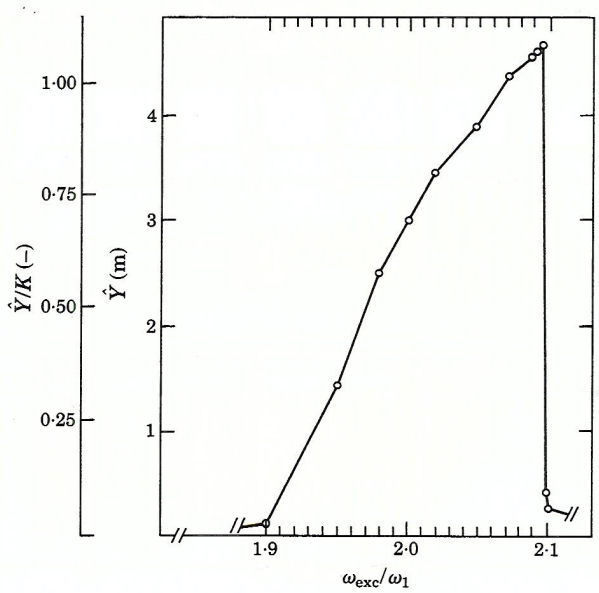

Figure 13. The shift of parametric resonance due to the increase of average tension. Details of Figure 8 around abscissa 2.

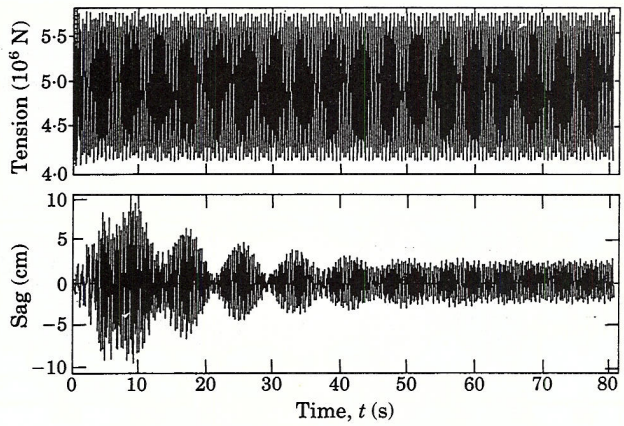

Figure 23. Resonance at $3\omega_1$. A three loops oscillation is observed.

(9) Some other excitations have been carried out to investigate the instability suggested by Labeeuw [8], when mixing of two frequencies is the excitation. This type of instability is more difficult to manage because of the relative value of the excitation amplitudes between the two frequencies. Therefore, many possibilities exist. It would be of some interest to generalize the theory to find new parameters which could replace k, ξ and a in that case. However in any case this type of instability is very dangerous from a practical point of view, because it is possible to have a wider range of dangerous frequencies which could be closer to a stay frequency (for example, if the two first frequencies of the bridge are 0·9 and 1·2, the first classical parametric resonances will occur at frequencies close to 0·45 and 0·6 Hz, and Labeeuw's resonances will occur at 0·15 and 1·05 Hz).

(10) It must be emphasized that a practical case would have a smaller amplitude than the corresponding one predicted by these simulations. This is because to obtain instability, in general one needs wind speed. If wind speed exists, there will be aerodynamic damping which will increase the damping, due to the non-conservative aerodynamic forces. This will be quantified in the next section.

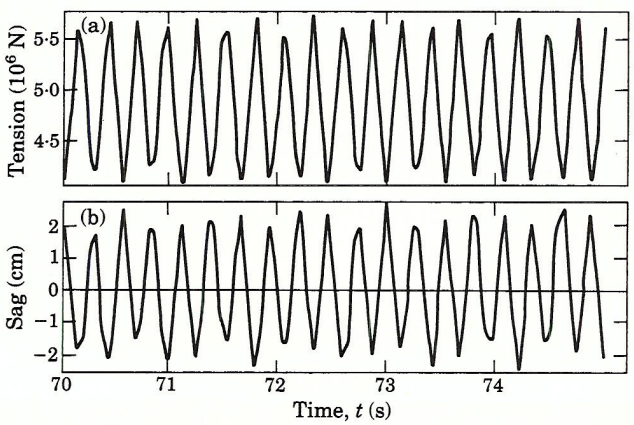

Figure 24. Details of Figure 23. (a) Tension time history; (b) mid-span displacement time history.

TABLE 1

Basic data for three typical stays of stayed bridges and corresponding peak-to-peak sag oscillation amplitudes during parametric oscillation of one end point, with amplitude X_d

	Stay 1	Stay 2	Stay 3
Cross-section (cm^2)	153	153	82·6
Tension (10^6 N)	8	8	4·9
Length (m)	440	50	110·5
Mass (kg/m)	133	133	64·8
Young's modulus (GPa)	190	190	210
Inclination (degrees)	17·5	60	Any (see below)
Damping (logarithmic decrement)	0·006	0·006	0·006
First frequency (Hz)	0·298	2·45	1·24
Irvine parameter, λ^2	1·77	0·006	0·0008
Initial sag (m) $= mgl^2 \cos\theta/8T_0$	3·84	0·05	0·20
Initial stretch, X_0 (m)	1·21	0·14	0·31
Threshold amplitude (mm), see equation (9)	4·62	0·53	1·18
Excitation amplitude, X_d (cm)	2, 5 and 10	2, 5 and 10	2, 5 and 10
Peak-to-peak sag oscillation (m)			
Computed by finite element code	n.c., 11·2 and 14·6	1·3, 2·1 and 2·96	1·5, 3·0 and 4·46
Calculated with Kovács formula	5·4, 8·44 and 11·9	1·8, 2·8 and 4·0	2·7, 4·2 and 6·0

The inclination has no influence on the result if the Irvine parameter is close to zero.
n.c. means "not computed".

7. APPLICATIONS TO SOME PRACTICAL CASES

As has been shown, the non-dimensional parameters used in Figure 6 provide access to any other cases: any length, any excitation amplitude—in short, any cable. One can suppose that parametric excitation at $2\omega_1$ is possible with corresponding bridges (this means that either girder or mast frequencies could satisfy this relationship, for any parametric resonance or Labeeuw ones), and that the logarithmic decrement is in the same range as the given values.

We have chosen two stays of the "Pont de Normandie" (stay 1 and 2) and one stay from the "Ben-Ahin" bridge (stay 3), to provide practical examples. The structural data and results are shown in Tables 1 and 2. It could be said that these amplitudes are in fact very large and very dangerous. Should they be dramatically reduced owing to aerodynamic damping?

TABLE 2

Range (max–min) *of tension oscillation* (10^6 N) *in the stays during the limit cycle of parametric oscillation and corresponding relative variation* $(T_{max} - T_{min})/T_0$ *in %*

	Excitation amplitude, X_d (cm)					
	2		5		10	
Stay 1	n.c.	n.c.	10·0–7·0	37·5%	10·7–7·0	78%
Stay 2	9·1–6·8	29%	11·0–5·9	63·8%	14·0–2·5	144%
Stay 3	5·25–4·53	14·7%	5·65–4·15	19%	6·5–3·0	71%

n.c. means "not computed".

19. W. SZEMPLIŃSKA-STUPNICKA 1978 *Journal of Sound and Vibration* **58**, 347–361. The generalized harmonic balance method for determining the combination resonance in the parametric dynamic systems.
20. T. IWATSUBO, Y. SUGIYAMA and S. OGINO 1974 *Journal of Sound and Vibration* **33**, 211–221. Simple and combination resonances of columns under periodic axial loads.
21. T. IWATSUBO, Y. SUGIYAMA and K. ISHIHARA 1972 *Journal of Sound and Vibration* **23**, 245–257. Stability and non-stationary vibration of columns under periodic loads.
22. H. M. IRVINE 1981 *Cable Structures*. Cambridge, Massachusetts: The M.I.T. Press.
23. H. M. IRVINE and T. K. CAUGHEY 1974 *Proceedings of the Regional Society, London* **A341**, 299–315. The linear theory of free vibrations of a suspended cable.
24. N. C. PERKINS 1992 *Journal of Sound and Vibration* **156**, 361–365. Discussion of "Dynamic stability of cables subjected to an axial periodic load".
25. L. LANDAU and E. LIFSHITZ 1978 *Fisica Teórica—Mecânica* 1. Moscow: Mir (in Russian).
26. *Norme Belge NBN N*03-002. Actions du vent sur les constructions.
27. J. L. LILIEN 1983 *Thèse de doctorat. Collection de publications de la Faculté des Sciences Appliquées de l'Université de Liège* 87. Constraintes et conséquences électromécaniques liées au passage d'une intensité de courant dans les structures en cables.
28. SAMCEF-CABLE 1991 Software for static and dynamic analysis of cable structures. Distributed by Samtech S.A., Bd Frère Orban 25, B4000 Liège, Belgium.
29. S. C. WATSON and D. STAFFORD 1988 *Civil Engineering, ASCE* **58**(4), 38–41. Cables in trouble.
30. D. W. JORDAN and P. SMITH 1987 *Nonlinear Ordinary Differential Equations*. Oxford: Oxford University Press, Applied Mathematics and Computing Science Series, second edition.
31. L. MEIROVITCH 1975 *Elements of Vibration Analysis*. New York: McGraw-Hill.

APPENDIX: LIST OF SYMBOLS

a ω_1/v, non-dimensional frequency
A cross-section of the cable (m^2)
E elasticity modulus of the cable (N/m^2)
K $=(4/\pi)\sqrt{X_0 l/3}$, reference amplitude
k $=b/\omega_1=\delta/\pi$, non-dimensional damping
l chord length of the cable (m)
m mass per unit of length of the cable (kg/m)
T_0 traction in the cable (component in the chord direction) (N)
Δx excitation amplitude (m); in our simulations we use only one sinusoidal component so that $\Delta x = X_d \sin 2vt$
X_d for cable stay (very low Irvine parameter λ) could be approximated by $X_d = \Delta Tl/EA = (T_{max} - T_0)l/EA$
X_0 initial stretch (m), which for cable stay (very low Irvine parameter λ) could be approximated by (X_0 is the difference between unstrained length and strained one with T_0) $X_0 = T_0 l/EA$
Y the cable displacement orthogonal to the chord
δ damping, expressed as logarithmic decrement
λ the Irvine parameter [1, 28] to determine if the cable behaviour is close to a weightless string (small value as for stay, implies sag/span ratio lower than 0·005) or not (large value as for overhead electrical lines, sag/span ratio in the range 0·02–0·04)
θ inclination of the cable span (0° is an horizontal cable)
ξ $=X_d/2X_0$ (X_0 is the initial applied stretch and X_d is the driving amplitude); in Figure 6 P is used, which is equivalent to 2ξ
v half of the excitation frequency ($v=\omega_1$ is the fundamental parametric excitation at twice the first mode cable frequency) (Hz)
ω_1 $=(\pi/l)\sqrt{T_0/m}$, first mode frequency of the cable (in plane frequency)